Rapid #: -12903488

CROSS REF ID: **318844**

LENDER: **MDU :: Health Sciences Library**

BORROWER: **ITD :: Eugene McDermott Library**

TYPE:	Article CC:CCG
JOURNAL TITLE:	Advanced Materials Technologies
USER JOURNAL TITLE:	Advanced Materials Technologies
ARTICLE TITLE:	A Novel Soft Actuator for the Musculoskeletal System
ARTICLE AUTHOR:	Wu, Lianjun
VOLUME:	19 FEB
ISSUE:	
MONTH:	19 FEB
YEAR:	2018
PAGES:	epub
ISSN:	2365-709X
OCLC #:	

Processed by RapidX: 2/20/2018 12:02:16 PM

ADVANCED MATERIALS TECHNOLOGIES
www.advmattechnol.de

A Novel Soft Actuator for the Musculoskeletal System

*Lianjun Wu, Indrajeet Chauhan, and Yonas Tadesse**

The musculoskeletal system (MS) is essential for the movements of biological systems. Inspired by this natural structure, several attempts are made to create a synthetic MS. However, one of the challenges in developing an artificial MS for biomimetic robots is the lack of a high-performance, low-cost, light-weight, and compact artificial muscle. In this Communication, a novel twisted and coiled artificial muscle is demonstrated, which is a promising actuator for the development of the artificial MS. The new muscle is made by twisting a nylon 6 fishing line precursor fiber and wrapping with a very thin (80 µm diameter) resistance wire. The resistance wire is not twisted during twist insertion of the polymer, which is very important for the performance of the muscle. The new muscle termed TCP^{FL}_{NC} is integrated in a 3D printed ball-and-socket-based artificial MS. Characterization results show a remarkable tensile actuation (53% strain provided at 1.69 MPa for an input current of 0.22 A). Furthermore, a bioinspired design and fabrication of the synthetic MS is illustrated incorporating antagonistic pairs capable of reaching a bending angle of 20° within 1 s. These actuators can potentially be used in other soft robots, prosthetics, and orthotics advancing the progress in the area.

The musculoskeletal system (MS) is a vital biological system that allows versatile movement of humans and other animals. Comprised of bones, muscles, tendons, ligaments, and other connective tissues,[1] the MS is actuated by the contraction of muscles to maneuver the skeleton that supports and protects the body. Various approaches of developing artificial MS using different actuator technologies, such as motors and pneumatic artificial muscles, have been demonstrated.[2–5] However, actuators like the electric motors and pneumatic artificial muscles have drawbacks for this application. Although electric motors are energy-efficient actuators, they require complex transmission system, resulting in limitations in terms of size and space. Above all, electric motors do not fit the bioinspired design approach. On the other hand, pneumatic artificial muscles require a compressor to force a gas into the actuators to create a pressure difference between the inside and the ambient environment for actuation. This makes the overall system of pneumatic artificial muscles bulky. The other major drawbacks are the requirement of solenoid valves and the large noise from the compressor during actuation. For an artificial musculoskeletal system, it is desirable to have a muscle-like actuator. In addition, large mechanical power output, good tensile actuation, and dynamic response are essential requirements for this application.

Twisted and coiled polymer (TCP) muscle from fishing line emerged as a promising actuator as shown in Haines et al.;[6] it can deliver a large strain of 49%, lift loads over 100 times heavier than those lifted by a human muscle of the same length and weight, generate 5.3 kW of mechanical work per kilogram of muscle weight, and undergo over 1 million life cycles. The fundamental mechanism in twisted and coiled actuator is the thermally induced fiber untwist in the coiled structure, which allows for both torsional and tensile actuation.[7,8] TCP muscle from fishing line can be actuated via hydrothermal actuation, but Joule heating is a convenient method because it eliminates a complicated actuator system like hot water reservoir and fluid pump needed for hydrothermal actuation.[9] However, as an inherently nonconductive material, actuation of TCP muscle from fishing line via electrothermal actuation is still a challenge. Different approaches have been proposed to add electrical conductors to artificial muscles, for instance, wrapping flexible carbon nanotube sheets,[6] coating nylon fishing line with conductive silver paint,[10,11] and twisting metal wire and fishing line simultaneously.[12–15] Metal wires used include copper, nickel-titanium shape memory alloy, iron, and nichrome, ranging from a diameter of 140 to 200 µm. Our unique approach is to wrap the resistance wire around the twisted fiber. This novel fabrication method can yield a better actuator for several reasons. First, it will enable the actuation of TCP muscle from fishing line (nonconductive) via electrothermal actuation (Joule heating). Second, avoiding twist to resistance wire enables the use of a very thin resistance wire of a diameter of 80 µm (tensile strength 690 MPa). If twist is inserted into the resistance wire, the thin resistance wire would break during the fabrication procedure. This is one of the main reasons why we avoid twisting the resistance wire. Third, the fabrication process using a very thin resistance wire will have negligible mechanical effect on the actuation. Lastly, the resistance of TCP muscle will no longer change significantly with the increase of temperature. Hereinafter, we refer to this actuator as TCP^{FL}_{NC} muscle.

Counterparts in nature serve as the best resource for inspiration and biomimicry for the design of an artificial MS. Given the unique biological significance of the ball-and-socket joint in a variety of species, we propose an artificial MS based on the ball-and-socket joint, which can serve as a biomimetic building block that can then be cascaded in various fashions to create

Dr. L. Wu, I. Chauhan, Prof. Y. Tadesse
Mechanical Engineering Department
The University of Texas at Dallas
800 W Campbell Rd, Richardson, TX 75080, USA
E-mail: yonas.tadesse@utdallas.edu

The ORCID identification number(s) for the author(s) of this article can be found under https://doi.org/10.1002/admt.201700359.

DOI: 10.1002/admt.201700359

advanced robots. The proposed MS consists of a 3D printed ball-and-socket joint, TCP_{NC}^{FL} muscles, a stabilization element made of silicone to serve as ligament, and a soft silicone layer to embed the entire structure and serve as a tissue surrounding the joint. TCP_{NC}^{FL} muscles make up the muscular system, whereas the ball-and-socket joint serves as the skeletal system for biomimetic robots. The typical joint angles of ball-and-socket joint in humans and other animals are less than 180°. In fact, adduction motion in such a joint for cats is 20–30°. The speed of such joints in most animals is in the range of 1–25 Hz (Table S1, Supporting Information). The joint presented in this Communication mimics the motion ranges of the seven cervical vertebrae of humans (C1–C7), which have a motion range of 2–36° and a maximum frequency of 1 Hz. The entire MS system is designed to actuate in a multidimensional fashion for ubiquitous use in robotics.

The TCP_{NC}^{FL} muscles were fabricated by the following four major steps: twist insertion, resistance wire wrapping, mandrel coiling, and thermal annealing (see the Supporting Information for detailed fabrication procedures), resulting in a uniform and extensive surface contact between the fishing line and resistance wire (**Figure 1**A). The fabricated muscle (Figure 1B) consists of an 860 µm diameter nylon 6 monofilament and an 80 µm diameter resistance wire. It has a spring index (the ratio of mean coil diameter to the fiber diameter) of 5.2 and the pitch of the nichrome is 0.877 mm. The muscle capability of lifting a 100-gram load (1.69 MPa) by 53% tensile actuation (input current 0.22 A, a duration of 6 s) is demonstrated in Figure 1C (Video S1, Supporting Information). This realized stroke is significant and can be useful in many applications in robotics where large actuation is required. TCP_{NC}^{FL} muscles were employed as contractile actuators for the joint in the four channels of the structure (Figure 1D) to provide multidimensional actuation. The channels are used primarily for insertion of the muscles and they can be used when needed for active cooling of the muscles. However, active cooling is beyond the scope of this study.

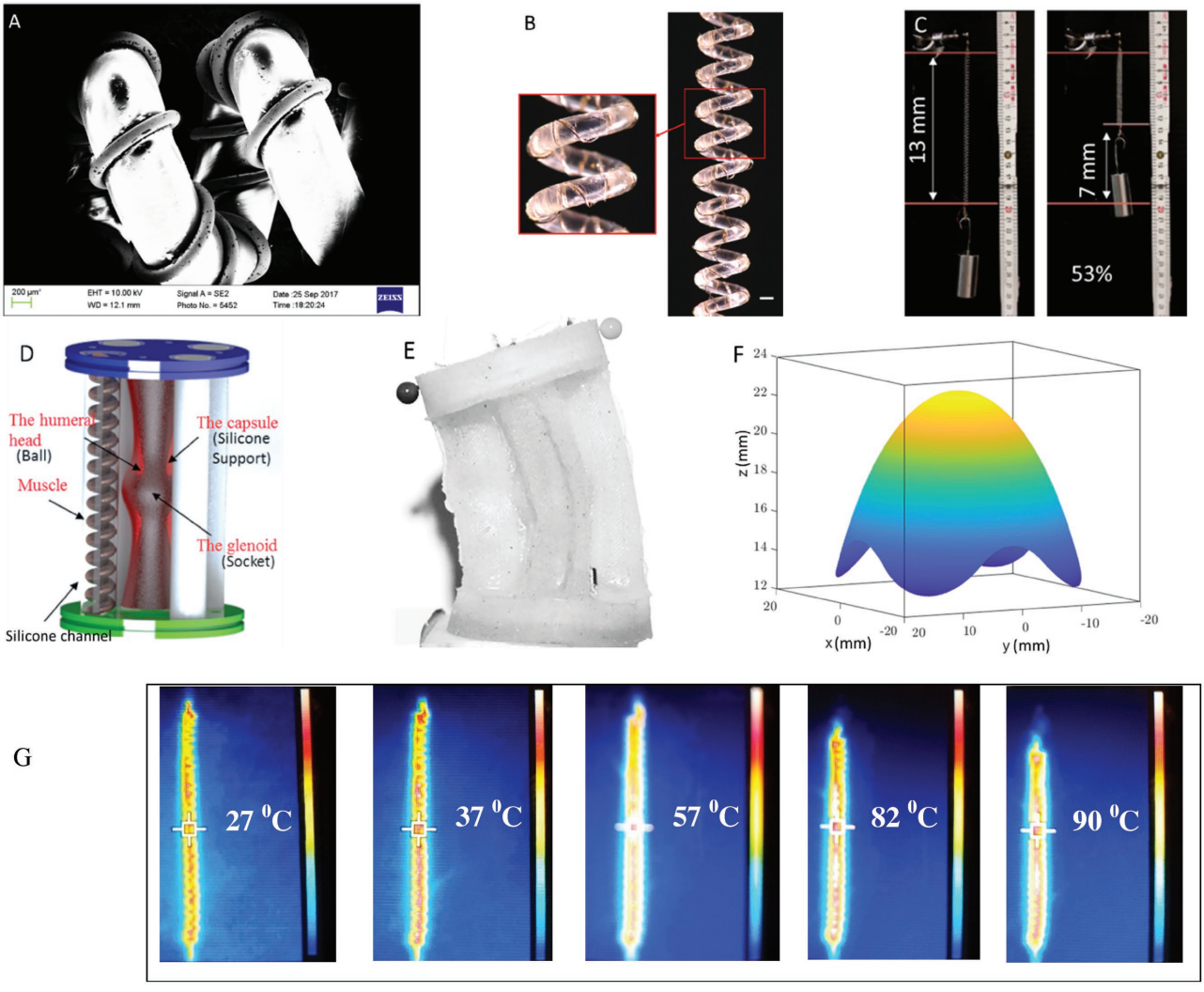

Figure 1. Muscle structure and integration in musculoskeletal system (MS). A) A scanning electron microscope image and B) optical images of TCP_{NC}^{FL} muscle. C) Electrothermal actuation of TCP_{NC}^{FL} muscle lifting a 100 g load by 53% actuation stroke. D) Schematic diagram of the MS based on ball-and-socket joint structure using bioinspired antagonistic pairs of muscles. E) The MS under actuated state. F) Dexterous workspace of the MS. G) The temperature distribution along the actuator's surface; the cursor indicates temperature at that spot.

Muscles of equal length were placed in antagonistic pairs to facilitate the relaxation of the actuated muscle. As the actuated muscle contracts, the opposing nonactuated muscle extends due to compliance and thereby stores energy to accelerate the relaxation of the actuated muscle. Figure 1E shows the final MS prototype, and Figure 1F provides a graphical visualization of the MS workspace (reachable positions of the joint). The reachable workspace of the MS is defined as all the positions that can be reached by any point on the outer circumference of the top moving plate with arbitrary muscles' actuation. The workspace can be determined numerically according to the position analysis (shown in the Supporting Information). To observe the temperature distribution, thermal imaging of the actuator was performed using an FLIR camera (TG165, FLIR Systems, Inc.). Figure 1G shows the temperature distribution of the muscle obtained from IR images corresponding to the temperature changes at the input current of 0.12 A. There is a slight difference in the temperature distribution along the surface at low temperature compared to high temperature. At low temperature (27 °C), the temperature is more uniformly distributed along the axial direction compared to high temperature (90 °C).

3D printing and casting were primarily used for manufacturing the MS. **Figure 2**A–G shows the fabrication in a step-by-step procedure. Because the existing advanced multimaterial 3D printer for soft materials cannot fabricate low shore hardness (below shore 26 A scale),[16] silicone molding technique has been widely used in creating soft actuators.[17,18] Therefore, we adopted silicone molding as a prime choice. The ball-and-socket joint and molds were 3D printed separately, as shown in Figure 2A, and then assembled for silicone casting as shown in Figure 2B, to create the stabilization elements and one pair of hollow channels (Ecoflex 00-10, Smooth-on Inc.; Figure 2C). The other pair of hollow channels was fabricated in a similar manner as shown in Figure 2D,E. To reinforce the connections between the hollow channels and the ball-and-socket joint, a silicone layer was fabricated at the top and bottom (Figure 2F,G).

The MS structure relies on the contraction of muscles that pull on the skeleton for versatile movement. While the pulling force and contraction of the muscles are critical parameters that affect the performance of the MS, the stiffness of the joint significantly affects the results as well. The stiffness of the MS joint and the muscle was characterized using the experimental setup as shown in Figure S2a (Supporting Information). A load cell (Futek LSB 200) and a laser displacement sensor (Keyence Lk-G152) were used to measure the force and displacement,

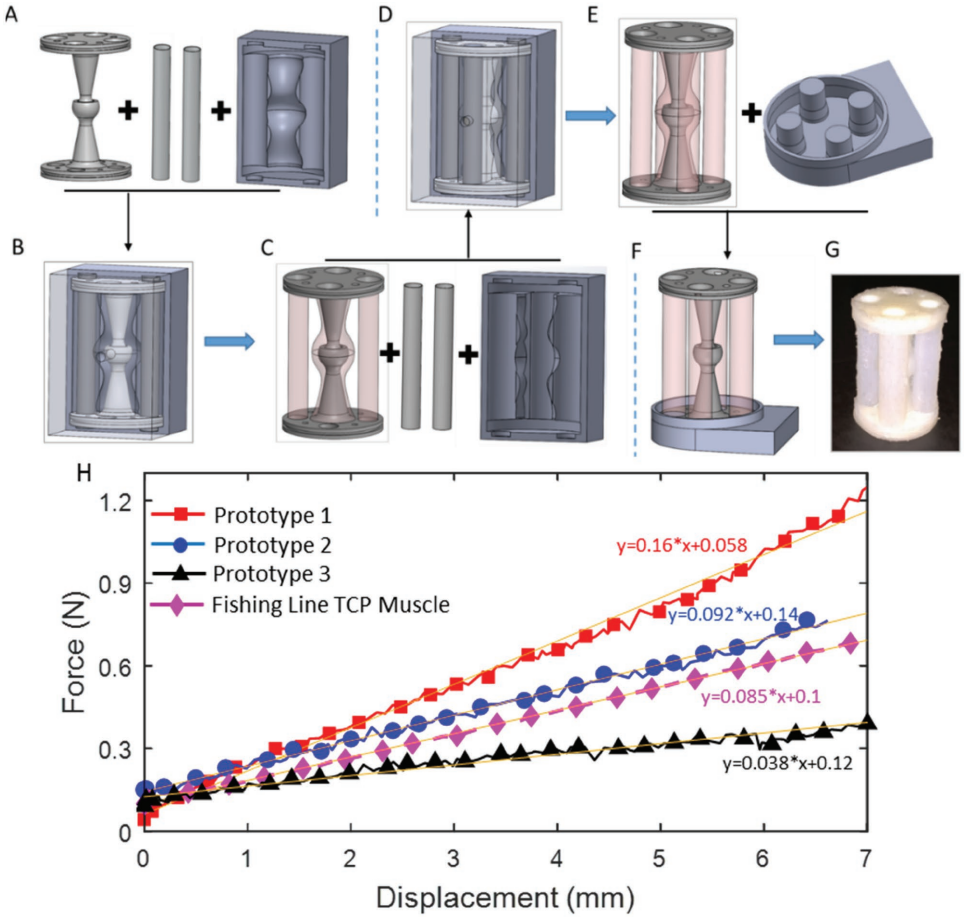

Figure 2. Fabrication and stiffness test of the ball-and-socket joint: the molds in (A) were 3D printed. The silicone ligament and one pair of channels were fabricated from steps (B) and (C). E) The other pair of channels were fabricated from step (D). F) Encapsulating the MS, a silicone layer was created to cover the top and bottom plates and secure the connection between four channels and the joint. G) The final fabricated prototype. H) The stiffness measurement of the MS and the muscle.

respectively. In this study, three different prototypes with a similar structure were fabricated. Figure 2H shows the results of the stiffness characterization of the joint structure (without integrating muscles). It can be seen that prototype 3, which has a joint stiffness of ≈40 N m^{-1}, requires the least effective force (0.04 N) to get the maximum bending motion (7 mm contraction displacement is required). Since the MS comprises a bioinspired antagonistic pair of muscles, the actuated muscle must overcome not only the stiffness of the joint but also the stiffness of the nonactuated muscle in the pair. Hence, the stiffness of the muscle is also of great interest. As shown by the magenta line in Figure 2H, the muscle stiffness is greater than that of prototype 3 and has an equivalent stiffness of 85 N m^{-1} (obtained from tensile test).

To gain insight into the mechanical performance of TCP_{NC}^{FL} muscles, the muscles driven by a square-wave input current (0.12 A, duty cycle 23%, and a period of 130 s) were characterized through isotonic and spring-load tests using the experimental setups as shown in Figure S3 (Supporting Information). For isotonic tests, **Figure 3**A shows the load dependence of absolute displacement, tensile actuation, loaded length, and temperature. The maximum absolute displacement occurred at a constant load of 30 g. The tensile actuation normalized to the loaded muscle length also depends mainly on the applied load as the muscle elongates considerably under higher load. The maximum tensile actuation, realized at a constant load of 30 g at a constant current of 0.12 A (duty cycle 23% and a period of 130 s), was 40% stroke. The loaded length is proportional to the applied loads. The maximum and minimum temperature remained at around 110° and 27°, respectively, as the current was kept constant all the time. One assumption for spring-load test is that the muscle integrated in the MS will work similarly against a linear spring with a stiffness of 125 N m^{-1} (the equivalent stiffness of the antagonistic nonactuated TCP_{NC}^{FL} muscle, 85 N m^{-1} and the joint structure, 40 N m^{-1}). In spring-load test, the performance of the same TCP_{NC}^{FL} muscle was measured at different

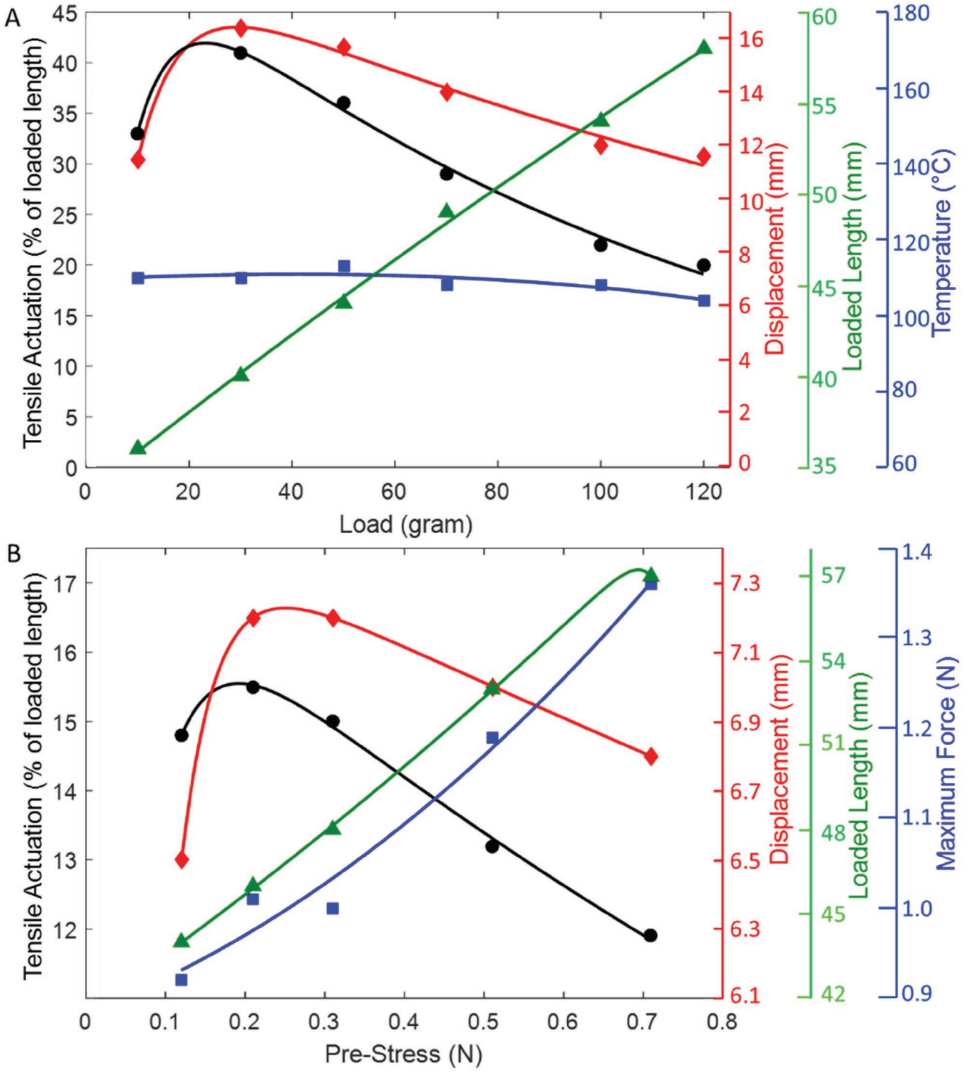

Figure 3. Average tensile actuation (percent of the loaded length), the absolute contraction displacement, the loaded length, temperature and maximum force of a TCP_{NC}^{FL} muscle. A) Isotonic test shows the graph at different load, and B) spring-load test shows the graph against a passive spring of stiffness of 133 N m^{-1} at different pre-stress values.

pretensions against a linear spring with a stiffness of 133N m^{-1}, which is slightly larger than the overall stiffness 125 N m^{-1}. The pretension was adjusted by translating the linear stage in discrete steps. Figure 3B illustrates the tensile actuation, contraction displacement, loaded length, and maximum pulling force at different pretension levels. The largest displacement (maximum actuation stroke) was obtained at pretension of 0.21 N (optimal pretension). All the state variables of TCP_{NC}^{FL} muscle (one cycle shown in **Figure 4**A,B and three cycles demonstrating consistency and repeatability shown in Figures S4 and S5, Supporting

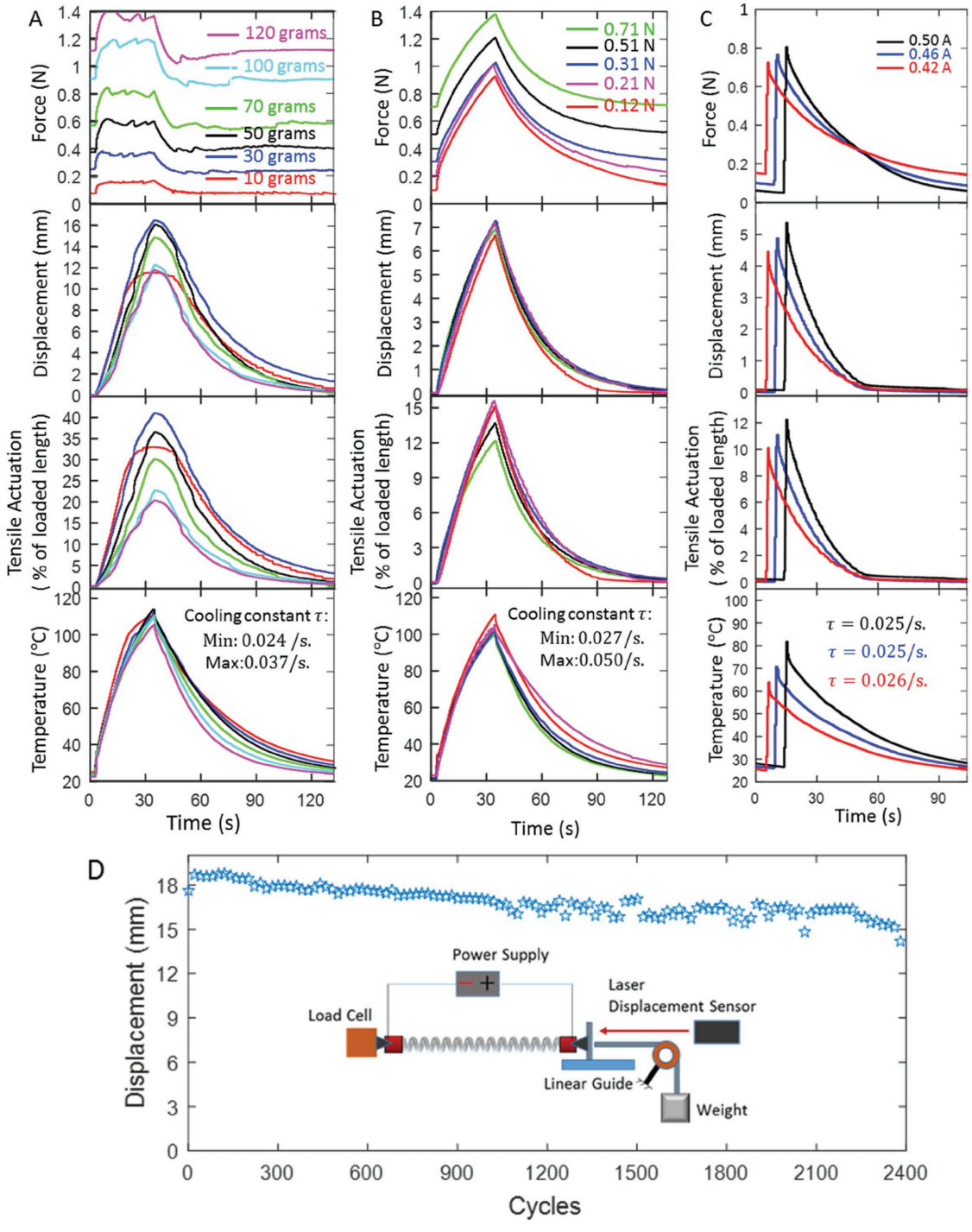

Figure 4. Time domain response of the force, displacement, tensile actuation, and temperature for TCP_{NC}^{FL} muscle under different power and load conditions. Results of A) isotonic test at different constant loads, B) spring-load test at different pretension magnitudes both at a square-wave input current, and C) spring-load test at variable pulsed current input. D) Life cycle test of the muscle driven by a pulsed current (0.5 A, duty cycle 1%, and a period of 101 s) under a constant 50 g load for 2300 cycles of actuation.

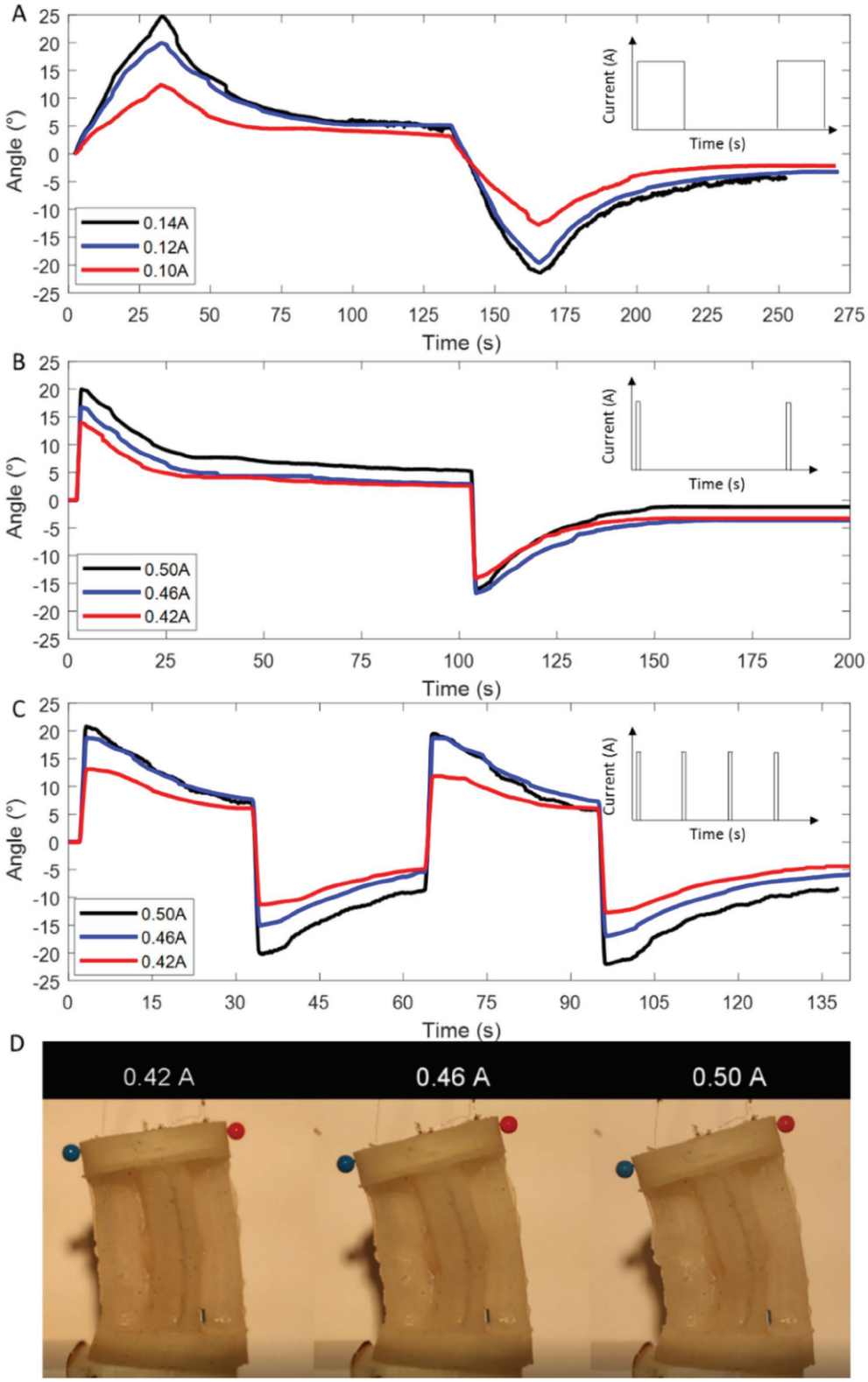

Figure 5. Characterization of the musculoskeletal system: A) MS bending motion at square wave at 23% duty cycle and a period of 130 s. B) Pulsed actuation at 1% duty cycle and a period of 101 s. C) Pulse actuation at 3.2% duty cycle and a period of 31s. D) The structure at the maximum bending angle at different current magnitude as shown in (C).

Information) including the pulling force, voltage, displacement, and temperature were measured synchronously and stored in the master PC. We also performed the blocking force measurement by using dead weights attached at the bottom of a muscle (resistance is around 150 Ω) until no corresponding tensile contraction was observed at a constant current of 0.12 A (input duration 30 s at 19 V maximum voltage). The blocking force was found to be 500 g (5 N), which is 1000 times its own weight. The mass of the muscle was 0.5 g including the crimps.

For the spring-load test, driving the same TCP_{NC}^{FL} using short pulse with high electrical current (0.42–0.50 A for 1 s) reveals high speed of actuation without sacrificing tensile actuation (Figure 4C). As shown in Figure 4C, a pulsed current input of 0.50 A for only 1 s results in 12% actuation stroke, which is nearly 80% of the maximum actuation stroke achieved by applying square-wave current input (0.12 A for 30 s at spring-load test in Figure 4B). The maximum pulling force of the muscle under the spring load at 0.50 A is 0.8 N. For endurance test, the muscle was driven by a pulsed current (0.5 A, duty cycle 1%, and a period of 101 s) for 2300 cycles continuously in ambient air (Figure S6, Supporting Information), and only a slight degradation of performance was observed (Figure 4D). From the temperature plots (Figure 4), the cooling time constants are determined for the cooling curves. These are obtained from Equation (S2) of the Supporting Information.

The characteristics of the MS were then analyzed after integration of the muscles (length 45 mm, outside diameter 4.5 mm, and an electrical resistance of 113 Ω). The MS was tested with three different currents ranging from 0.10 to 0.14 A at an increment of 0.02 A (duty cycle 23% and a period of 130 s), equivalent power of 1.1–2.2 W. **Figure 5**A shows that the different angular displacements were obtained at different constant currents and the maximum angular displacement was ≈24°. The pulsed actuation tests were performed to increase the operation frequency of the MS. Figure 5B shows the angular displacement at pulsed actuation with higher currents (duty cycle 1% and a period of 101 s), where the maximum angular displacement was ≈21°. One benefit of implementing the antagonistic pair of muscles is the increase in frequency due to the reduced relaxation time. Figure 5B shows one bending motion without the antagonistic muscle turned on during the period from 0 to 105 s; however, the antagonistic muscle in Figure 5C was turned on at the 34th s. Due to the actuation of antagonistic muscle in Figure 5C (Video S2, Supporting Information), the relaxation time was reduced to 30 s in Figure 5C from 100 s as shown in Figure 5B. The continuous cycle test in Figure 5C also reveals a consistent and repeatable mechanical performance. During the pulsed actuation test, the frequency of the MS was increased from 8 mHz (Figure 5A) to 30 mHz (Figure 5C) or by a factor of 3.75 (Video S3, Supporting Information). This is a significant improvement from our previous joint, which broadens the scope for practical implementation. Figure 5D shows the structure at the maximum bending angle at different current magnitude as shown in Figure 5C. Using a geometrical relationship that correlates the bending angle and the muscle contraction,[19] the tensile actuation obtained in spring-load test (Figure 4) and bending angles (Figure 5) are well correlated. There is a slight difference between the two tests due to a slight variation in stiffness. The design enables further improvements in frequency by reducing the relaxation time. Besides utilizing the antagonistic pairs of muscles, active cooling of the muscles is another important aspect to improve the response of the MS. Specifically, the addition of silicone channels around the muscles allows for implementation of different methods of both active and passive cooling, which will be carried out and discussed in future study. For instance, the frequency can be increased via active cooling by incorporating pumps to enable the flow of a fluid to quench the muscles. However, there are some issues to be addressed regarding the active cooling in the future study, such as the effect of the stiffness of the piping on the performance of MS, the sealing of the silicone channels, and the type of fluid to use. We will investigate those issues and intend to report them in the future.

Here, we have shown a polymer artificial muscle from fishing line and resistance wire following a new method. We achieved a remarkable improvement in the performance of TCP muscles (53% provided at 1.69 MPa) compared with the one reported in the reference (49% tensile contraction provided at 1 MPa).[6] Moreover, we demonstrated a bioinspired design of artificial musculoskeletal system powered by the novel high-performance, and extremely low-cost TCP_{NC}^{FL} muscles. The novel TCP_{NC}^{FL} muscle shows great potential in soft robots' application where tremendous displacement, large force, and compact size are required. The combination of TCP_{NC}^{FL} muscle and modular 3D printed joints has potential applications in many robotic systems, such as snake robots, underwater manipulator, and underwater swimming robots.

Supporting Information

Supporting Information is available from the Wiley Online Library or from the author.

Acknowledgements

The authors would like to acknowledge the support of the Office of Naval Research (ONR), Young Investigator Program, under Grant No. N00014-15-1-2503.

Conflict of Interest

The authors declare no conflict of interest.

Keywords

artificial muscles, bioinspiration, musculoskeletal systems, robotics, smart actuators

Received: December 4, 2017
Revised: December 31, 2017
Published online:

[1] L. Ren, Z. Qian, L. Ren, *J. Bionic Eng.* **2014**, *11*, 159.
[2] C. Richter, S. Jentzsch, R. Hostettler, J. A. Garrido, E. Ros, A. Knoll, F. Rohrbein, P. van der Smagt, J. Conradt, *IEEE Robot. Autom. Mag.* **2016**, *23*, 128.

[3] S. Kurumaya, K. Suzumori, H. Nabae, S. Wakimoto, *ROBOMECH J.* **2016**, *3*, 18.
[4] S. Ikemoto, Y. Kimoto, K. Hosoda, *Bioinspiration Biomimetics* **2015**, *10*, 066009.
[5] D. Yang, M. S. Verma, J. H. So, B. Mosadegh, C. Keplinger, B. Lee, F. Khashai, E. Lossner, Z. Suo, G. M. Whitesides, *Adv. Mater. Technol.* **2016**, *1*, 1600055.
[6] C. S. Haines, M. D. Lima, N. Li, G. M. Spinks, J. Foroughi, J. D. Madden, S. H. Kim, S. Fang, M. J. de Andrade, F. Göktepe, *Science* **2014**, *343*, 868.
[7] J. Di, S. Fang, F. A. Moura, D. S. Galvão, J. Bykova, A. Aliev, M. J. de Andrade, X. Lepró, N. Li, C. Haines, *Adv. Mater.* **2016**, *28*, 6598.
[8] J. A. Lee, N. Li, C. S. Haines, K. J. Kim, X. Lepró, R. Ovalle-Robles, S. J. Kim, R. H. Baughman, *Adv. Mater.* **2017**, *29*, 1700870.
[9] L. Wu, M. J. de Andrade, R. S. Rome, C. Haines, M. D. Lima, R. H. Baughman, Y. Tadesse, *Proc. SPIE* **2015**, *9431*, 94310I.
[10] S. M. Mirvakili, I. W. Hunter, *Adv. Mater.* **2017**, *29*, 1604734.
[11] S. M. Mirvakili, A. R. Ravandi, I. W. Hunter, C. S. Haines, N. Li, J. Foroughi, S. Naficy, G. M. Spinks, R. H. Baughman, J. D. Madden, presented at *SPIE Smart Structures and Materials + Nondestructive Evaluation and Health Monitoring*, San Diego, California, USA, March **2014**.
[12] A. N. Semochkin, presented at *2016 IEEE Int. Symp. on Assembly and Manufacturing (ISAM)*, Fort Worth, TX, USA, Aug. **2016**.
[13] C. Xiang, H. Yang, Z. Sun, B. Xue, L. Hao, M. A. Rahoman, S. Davis, *Smart Mater. Struct.* **2017**, *26*, 037004.
[14] J. van der Weijde, B. Smit, M. Fritschi, C. van de Kamp, H. Vallery, *IEEE/ASME Trans. Mechatronics* **2017**, *22*, 1268.
[15] T. Arakawa, K. Takagi, K. Tahara, K. Asaka, presented at *SPIE Smart Structures and Materials + Nondestructive Evaluation and Health Monitoring,* Las Vegas, Nevada, USA, April **2016**, p. 97982W.
[16] C. Kundera, J. Bochnia, *Rapid Prototyping J.* **2014**, *20*, 533.
[17] E. T. Roche, R. Wohlfarth, J. T. Overvelde, N. V. Vasilyev, F. A. Pigula, D. J. Mooney, K. Bertoldi, C. J. Walsh, *Adv. Mater.* **2014**, *26*, 1200.
[18] B. Gorissen, D. Reynaerts, S. Konishi, K. Yoshida, J. W. Kim, M. De Volder, *Adv. Mater.* **2017**, *29*, 1604977.
[19] L. Wu, Y. Tadesse, presented at *ASME 2016 Int. Mechanical Engineering Congress and Exposition,* Phoenix, Arizona, USA, November **2016**.